Nano Energy 62 (2019) 275–281

Contents lists available at ScienceDirect

Nano Energy

journal homepage: www.elsevier.com/locate/nanoen

Full paper

Diethyl ether as self-healing electrolyte additive enabled long-life rechargeable aqueous zinc ion batteries

Weina Xu[a,b], Kangning Zhao[a,c,d], Wangchen Huo[b], Yizhan Wang[a], Guang Yao[a], Xiao Gu[b], Hongwei Cheng[a], Liqiang Mai[d], Chenguo Hu[b,*], Xudong Wang[a,**]

[a] Department of Materials Science and Engineering, University of Wisconsin−Madison, Madison, WI, 53706, United States
[b] Department of Applied Physics, State Key Laboratory of Power Transmission Equipment & System Security and New Technology, Chongqing University, Chongqing, 400044, PR China
[c] College of Sciences & Institute for Sustainable Energy, Shanghai University, Shanghai, 200444, PR China
[d] State Key Laboratory of Advanced Technology for Materials Synthesis and Processing, International School of Materials Science and Engineering, Wuhan University of Technology, Wuhan, 430070, PR China

ARTICLE INFO

Keywords:
Zinc ion battery
Electrolyte additive
Zinc metal
Dendrite suppression

ABSTRACT

Aqueous rechargeable zinc ion batteries (ARZIBs) is considered one of the most compelling candidates for grid-scale energy storage owing to their cost effectiveness, good safety, eco-friendliness, high output voltage, and high capacity. However, their practical applications are still largely limited by the undesirable cyclability and high-rate capability. Here, we report a discovery that using a small amount (2 vol%) of diethyl ether (Et_2O) as the electrolyte additive could largely improve the performance of Zn–MnO_2 batteries. The addition of Et_2O yielded the first cycle coulombic efficiency of 95.6% at 50 mA/g, a high capacity of 115.9 mAh/g at 5 A/g and 97.7% retention of initial capacity after 4000 cycles, demonstrating an outstanding rate capability and cycling performance among the reported Mn-based zinc ions batteries in mild electrolyte. Ex-situ characterizations revealed that appropriate amount of Et_2O molecules could effectively suppress the formation of Zn dendrites on Zn anode, which is the main mechanism for cyclability improvements.

1. Introduction

Aqueous rechargeable multivalent-ion batteries are considered as a promising alternative for rechargeable lithium ion batteries (LIBs) due to their high volumetrical capacity, excellent safety, and low cost particularly for stationary storage systems [1–4]. Among a number of multivalent metal ions choices, zinc holds outstanding practical merits with a high volumetrical capacity of 5851 mAh/mL, a suitable negative potential of −0.762 V versus standard hydrogen electrode (SHE), and a high overpotential against hydrogen evolution [5,6]. As a result, aqueous rechargeable zinc ion battery (ARZIB) has received increasing research interests in recent years as a promising candidate for grid-scale energy storage [7,8]. However, the poor reversibility and low plating/stripping Coulombic efficiency (CE) of Zn anodes still challenge its practical application potential and remain largely unexplored [9–11]. As a result of the highly dynamic Zn/electrolyte interface [12,13], the main failure mechanisms of zinc anodes are dendrite formation and a high degree of corrosion. A smooth surface morphology of Zn anodes during cycling is thus considered to be crucial to achieve high cycling stability [13–15]. Various strategies have been implemented to suppress the corrosion and dendritic formation on Zn anodes. Typically, introducing a protection layer, such as an ultrathin TiO_2 film [16] and a nanoporous $CaCO_3$ coating [17], has been revealed as an effective strategy to impede the dendrite growth, leading to long life ARZIB. Three-dimensional (3D) Zn architecture has been also shown to be able to eliminate dendrite formation by minimizing the shape change [18,19]. Besides, alloying zinc with other metal elements could yield a more homogeneous surface potential on zinc and thus suppress the dendrite formation [20]. Nevertheless, despite the initial successes, these strategies all faces large technical hurdles for practical and scalable fabrications [21].

Alternatively, electrolyte additives have been intensively studied in LIBs as an effective approach to stabilizing the solid electrolyte interphase and eliminating the dendrite formation, resulting in improved cycling performance [22,23]. It has been found that selected electrolyte additive could be absorbed near the tip of lithium substrate surface

* Corresponding author.
** Corresponding author.
E-mail addresses: hucg@cqu.edu.cn (C. Hu), xudong.wang@wisc.edu (X. Wang).

https://doi.org/10.1016/j.nanoen.2019.05.042
Received 29 April 2019; Received in revised form 14 May 2019; Accepted 14 May 2019
Available online 15 May 2019

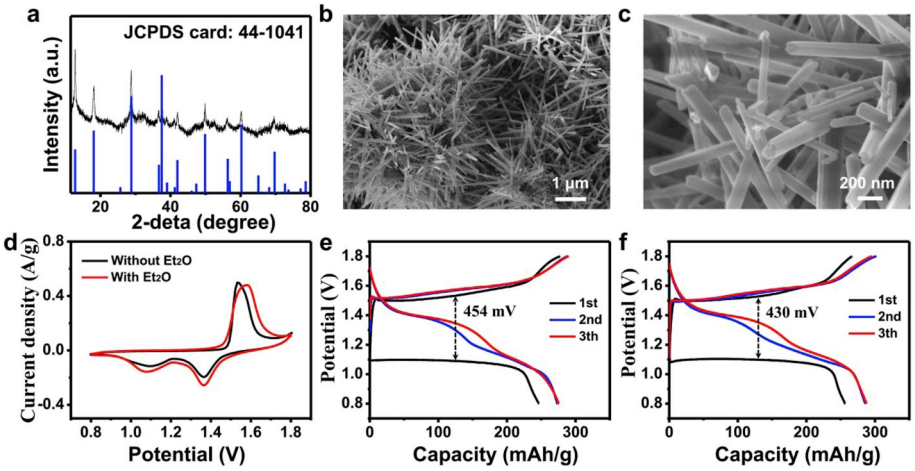

Fig. 1. Structural and electrochemical characterizations of MnO_2: a, XRD pattern of as-synthesized α-MnO_2 nanorods in comparison to the standard pattern (JCPDS card no. 44–1041). **b,** SEM images of as-synthesized α-MnO_2 nanorods. **c,** High-magnification SEM image revealing the size and geometry of α-MnO_2 nanorods. **d,** CV curves (the third cycle) at a scan rate of 0.1 mV/s for Zn–MnO_2 battery in aqueous electrolyte without and with Et_2O additive. **e** and **f,** Galvanostatic charge-discharge curves of the initial three cycles at current density of 50 mA/g in aqueous electrolyte without (e) and with (f) Et_2O additive.

forming an electrostatic shield, and suppress the dendrite formation by forming a smooth deposition layer [23]. Based on these observations, we expect that electrolyte additives might also play an important role in dendrite suppression for ARZIB. Considering diethyl ether (Et_2O) has been a popular electrolyte solvent that can effectively suppress lithium dendrites even at high charge rates, we hypothesize Et_2O may also serve as a promising additive for ARZIBs [24]. Herein, we reported an intriguing discovery that adding a very small amount of Et_2O in the aqueous electrolyte of ARZIB could largely suppress the dendrite formation on zinc anode during cycling, and thereby significantly improve the battery performance. By introducing 2 vol% Et_2O to the aqueous electrolyte, Zn–MnO_2 battery demonstrated an outstanding cycling performance with a high capacity retention of 97.7% for 4000 cycles at 5 A g^{-1}. This enhancement was attributed to the preferential adsorption of Et_2O on the high-potential dendrite tips, which could reduce the dendrite growth rate. This discovery could be a general and scalable strategy for improving the long-term performance of rechargeable aqueous battery systems.

2. Experimental section

2.1. Preparation of MnO_2 cathode

MnO_2 was synthesized by a hydrothermal method. In a typical procedure, 0.45 g of $KMnO_4$ and 1 mL of concentrated HCl (37%) were dissolved in 40 mL of deionized water and stirred for 20 min. Subsequently, the mixture was transferred into a 50 mL Teflon-lined stainless-steel autoclave and kept at 160° C for 12 h. Finally, the product was obtained after washing with deionized water/alcohol for six times and dried at 60° C overnight.

2.2. Structural characterizations

XRD were performed by a Bruker D8 Advance X-ray diffractometer with an area detector, using Cu Kα radiation (λ = 1.5418 Å). SEM images were recorded from a JEOL-7100F field-emission SEM (FESEM). X-ray photoelectron spectroscopy (XPS) spectrum was obtained from a Thermo Scientific K-alpha XPS instrument with a 100 μm spot size, with the flood gun turned on during the measurements.

2.3. Electrochemical characterizations

Zn–MnO_2 battery was assembled in CR2016 coin cells using a MnO_2 electrode as the cathode, glass fiber as the separator, and metallic Zn foil as the anode. The MnO_2 electrode was composed of α-MnO_2 nanorod powder as the active material, super P conductive additive, and polyvinylidene difluoride (PVDF) binder in a weight ratio of 7:2:1. The mass loading of active material was 3.5 mg/cm^2 3 M $Zn(CF_3SO_3)_2$ with 0.1 M $Mn(CF_3SO_3)_2$ mixed aqueous solution was chosen as the electrolyte. Et_2O (purity ≥ 99.0%) was used as the electrolyte additive with variable amounts. The presence of $Mn(CF_3SO_3)_2$ in the electrolyte could compensate the dissolution equilibrium of Mn^{2+} from the MnO_2 electrode and stabilize the electrode. Galvanostatic cycling performance at different current density was performed on a Lanhe-2100 battery tester. Cyclic voltammogram was conducted on Autolab PGSTAT302 N potentiostat in the voltage range of 0.8–1.8 V at a scan rate of 0.1 mV/s. Electrochemical impedance spectroscopy was obtained from an Autolab PGSTAT302 N in the frequency range of 10^{-2}-10^5 Hz at an open circuit condition.

A symmetrical Zn–Zn battery was assembled in CR2016 coin cells using Zn foil as both cathode and anode, 3 M $Zn(CF_3SO_3)_2$ as the electrolyte without/with 2 vol% Et_2O additive. Galvanostatic cycling of Zn–Zn battery was recorded on Lanhe-2100 battery tester. The corrosion of Zn foil was characterized by linear sweeping voltammogram at a sweeping rate of 1 mV/s, using the three-electrode configuration with Zn plate as the working electrode, Pt foil as the counter electrode, and saturated Ag/AgCl electrode as the reference electrode on an Autolab PGSTAT302 N.

3. Results and discussion

The α-MnO_2 nanorods were synthesized by a facile hydrothermal method following the literature [25]. The XRD pattern in Fig. 1a showed that all characteristic peaks matched well with a standard crystalline phase of α-MnO_2 (JCPDS: 44–1041) and no impurity peaks were observed. The XPS spectra revealed two Mn 2p peaks, located at 642.1 eV and 653.7 eV (Fig. S1), corresponding to the spin orbital of Mn 2p3/2 and Mn 2p1/2, respectively [26,27]. The spin-energy separation of these two peaks was 11.8 eV, suggesting that the valence state of the Mn ion was +4 in the as-prepared α-MnO_2 nanorods. The SEM image showed that the α-MnO_2 nanorods were bundled together with a high density (Fig. 1b). All the nanorods had a relatively uniform quasi-1D geometry with an average diameter of ~100 nm (Fig. 1c). These nanorods were directly used in the fabrication of Zn–MnO_2 ARZIBs.

Initially, to optimize the amount of Et_2O additive, the corrosion overpotential of Zn foil in 3 M $Zn(CF_3SO_3)_2$ electrolyte with different ratio of Et_2O in the electrolyte was evaluated in a three-electrode configuration with a Zn plate as the working electrode, a Pt foil as the counter electrode, and a saturated Ag/AgCl electrode as the reference electrode. It was found that 2 vol% Et_2O additive had the lowest overpotential (Fig. S2 and Table S1). The electrochemical impedance spectroscopy (EIS) analysis was conducted on fresh Zn–MnO_2 cells with different volume concentrations of Et_2O (Figs. S3a–b) to study the charge transfer at the electrode/electrolyte interface. The equivalent

circuit used for fitting the experimental EIS data was shown in Fig. S3c, in which R_s represents the ohmic resistance and R_{ct} represents the charge-transfer resistance at the electrode/electrolyte interface, respectively. The R_s value showed a very small variation when the amount of Et_2O was changed in the electrolyte. The R_{ct} value clearly evolved in a volcano curve (Fig. S3d) and the cell with 2 vol% Et_2O additive showed the lowest R_{ct} of 351 Ω. Therefore, 2 vol% Et_2O was used as the standard sample in remaining experiments.

The cyclic voltammetry (CV) profiles of Zn–MnO_2 batteries with and without Et_2O as an additive were compared to investigate the influence of Et_2O on the Zn–MnO_2 battery (Fig. 1d). Both CV curves exhibited similar redox pairs, suggesting that Et_2O did not affect the redox reaction of the MnO_2 cathode. During the cathodic sweep, two redox peaks were detected at around 1.36 and 1.1 V, which could be attributed to stepwise electrochemical Zn-insertion into α-MnO_2, while the appearance of the overlapped anodic peak was assigned to Zn-extraction from the cathode, which was in good agreement with previous reports [28,29]. More importantly, at 1.8 V, the current was slightly lower after adding Et_2O, which was consistent with the observed higher overpotential of zinc plate against hydrogen evolution. The galvanostatic charge/discharge (GCD) profiles of both Zn–MnO_2 batteries at a low current density of 50 mA/g showed a similar plateau (Fig. 1e, and f), which confirmed that Et_2O additive did not participate in any redox reaction of the Zn–MnO_2 battery. Interestingly, the Zn–MnO_2 battery showed a voltage difference between first and second discharge curves, which also had been seen in other ARZIB [30]. This phenomenon was on account of some thermodynamic factors, such as the volume and surface energy variations of MnO_2 cathode after charging [31,32]. And the Zn–MnO_2 battery without Et_2O had a nontrivial overpotential of ~454 mV in the initial cycle, while the overpotential decreased to 430 mV with the addition of Et_2O. In addition, the battery with Et_2O exhibited a discharge capacity of 257.3 mAh/g in the first cycle with an initial CE of 95.6%, much higher than those without Et_2O (245.4 mAh/g and 87.3%, respectively). In the subsequent two cycles, the discharge capacities of the battery with Et_2O increased to 285.6 and 288.0 mAh/g, respectively, approaching the theoretical value of MnO_2 (308 mAh/g based on single electron transfer between Mn^{4+}/Mn^{3+} redox pair).

The charge/discharge curves at different current densities were further investigated to compare the performance of Zn–MnO_2 battery with and without Et_2O (Fig. 2a and Fig. S4a). The corresponding rate capabilities were given in Fig. 2b and Fig. S4b, respectively. The Zn–MnO_2 battery with Et_2O delivered a reversible capacity of 284.0 mAh/g at 0.1 A/g. When the current was increased to 5.0 A/g, a capacity of 115.9 mAh/g was still retained. When the current density was switched back to 0.1 A/g, a capacity of 282.7 mAh/g was obtained, corresponding to a very high recovery rate of 98.9%. As a comparison, the same battery without Et_2O only delivered a capacity of 78.2 mAh/g at 5 A/g and achieved 88.3% of the initial capacity when the current density was recovered to 0.1 A/g. This Zn–MnO_2 battery with Et_2O outperformed previously reported Mn-based ARZIBs in mild aqueous electrolyte in terms of the rate capability, as displayed in Fig. 2c [16,33–43] and Table S2.

The influence of Et_2O on cycling stability of Zn–MnO_2 battery was further investigated. The battery with Et_2O delivered a reversible capacity of 274.3 mAh/g after 200 cycles at 0.3 A/g and 231.4 mAh/g after 300 cycles at 1 A/g, respectively (Fig. 2d), both of which exhibited high capacity retentions of 100%. In comparison, the battery without Et_2O only delivered 75.7% and 80.1% of its initial capacity at 0.3 A/g and 1 A/g, after 200 cycles, respectively (Fig. S5). The ultra-high capacity retention of our Zn–MnO_2 battery with Et_2O at low discharge current was superior to other reported Mn-based ARZIBs in mild aqueous electrolyte (Table S3). In addition, the CE at 0.3 A/g was also improved by adding Et_2O, which was approaching 100% after 45 cycles, but was only 96% without the additive. The long-term cycling stability was further tested at 5 A/g (Fig. 2e). The reversible capacity was retained at 113 mAh/g, corresponding to an outstanding capacity retention of 97.7% after 4000 cycles. In contrast, the capacity of the battery without Et_2O only stabilized at 71.8 mAh/g and failed after 1950 cycles (Fig. S6). Compared to the Mn-based ARZIBs reported so far, our Zn–MnO_2 battery with Et_2O demonstrated a superior cycling performance with a high discharging current in mild aqueous electrolyte (Table S4). Our results confirmed that adding Et_2O as the electrolyte additive could substantially improve the electrochemical performance of Zn–MnO_2 batteries in terms of rate capability and cycling stability. We also compared the Zn–MnO_2 battery with different ratios of Et_2O in the electrolyte at 3 A/g (Fig. S7). The results further confirmed that 2 vol% Et_2O in the electrolyte was the most favorable ratio for improving the cycling performance. It was discovered that the batteries with 1 vol% Et_2O and without additive both showed the leakage of electrolyte, implying that the corrosion of the zinc anode was severe (Fig. S8). In addition, we tested the cycling stability of Zn–MnO_2 batteries in 3 M $ZnSO_4$ and 0.1 M $MnSO_4$ aqueous electrolyte at 5 A/g (Fig. S9). Not surprisingly, adding 2 vol% Et_2O in this electrolyte also could significantly improve the cycling performance of Zn–MnO_2 battery.

To understand the role of Et_2O additive, we first performed ex-situ XRD and SEM analyses on both cathode and anode materials after 200 charge/discharge cycles at 0.3 A/g. For the MnO_2 cathode material, XRD of the fully discharged MnO_2 cathode with and without Et_2O showed the same pattern (Fig. S10), suggesting the phase transformation of the cycled MnO_2 was unchanged in the presence of Et_2O [35,39,44]. SEM images further showed that the morphology of the cycled MnO_2 cathodes had no distinguishable difference with and without Et_2O (Fig. S11).

As for the Zn anode, ex-situ XRD patterns confirmed that the deposited layer during Zn stripping/platting mainly consisted of Zn metal (JCPDS No. 04–0831) and no other impurities could be observed (Fig. S12), which agreed with the reported results of other Zn–MnO_2 batteries [33]. SEM images revealed that the Zn anode without Et_2O in electrolyte had a flake-like surface feature after cycling (Figs. S13a and b). However, this structural feature was not observed from the cycled Zn plate with Et_2O additive (Figs. S13c and d), which was much closer to the pristine zinc plate surface (Fig. S14). The obvious morphological difference evidenced that Zn dendrite formation was greatly suppressed by adding Et_2O.

Based on the ex-situ analyses, it was reasonably to hypothesize that the main effect of Et_2O was protecting the Zn anode during cycling, and it had negligible influence on the cathode material. Thus, to further shed light on the protection effect of Et_2O on Zn anode, a Zn–Zn symmetric configuration was studied using 3 M $Zn(CF_3SO_3)_2$ as the electrolyte with/without 2 vol% Et_2O. Fig. 3a showed a comparison of the cycling stability of Zn–Zn batteries with and without Et_2O at a current density of 0.2 mA/cm^2. The cell with Et_2O showed excellent stability and reversibility during the entire Zn plating/stripping processes. The voltage profiles of Zn–Zn batteries at different cycle number were enlarged for better recognition (Fig. 3b). The polarization of the battery with Et_2O at the 4th cycle was reduced from the initial 44 mV and kept at ~30 mV over the entire 125 testing cycles. In contrast, the battery without Et_2O showed a significant voltage fluctuation for Zn plating/stripping. Particularly, the polarization at 85th cycle suddenly increased and the voltage hysteresis exhibited sharp jumps up to 2.3 V. Such a high polarization could lead to battery death as the theoretical deposition/stripping potential was 0 V *vs.* Zn/Zn^{2+}. When the hysteresis went above 600 mV, the cell was regarded as failure. During the entire cycling process, the polarization of the battery with Et_2O was generally lower than that without Et_2O. Even at a high current density of 1 mA/cm^2, the Zn–Zn battery with Et_2O also exhibited a lower polarization of ~44 mV during cycling, whereas the cell without Et_2O exhibited a rising and fluctuating voltage hysteresis and failed at ~46 cycle (Fig. S15).

The EIS spectra of the Zn plates before and after the cycling test all showed only one semi-circle, suggesting a simple charge transfer at the

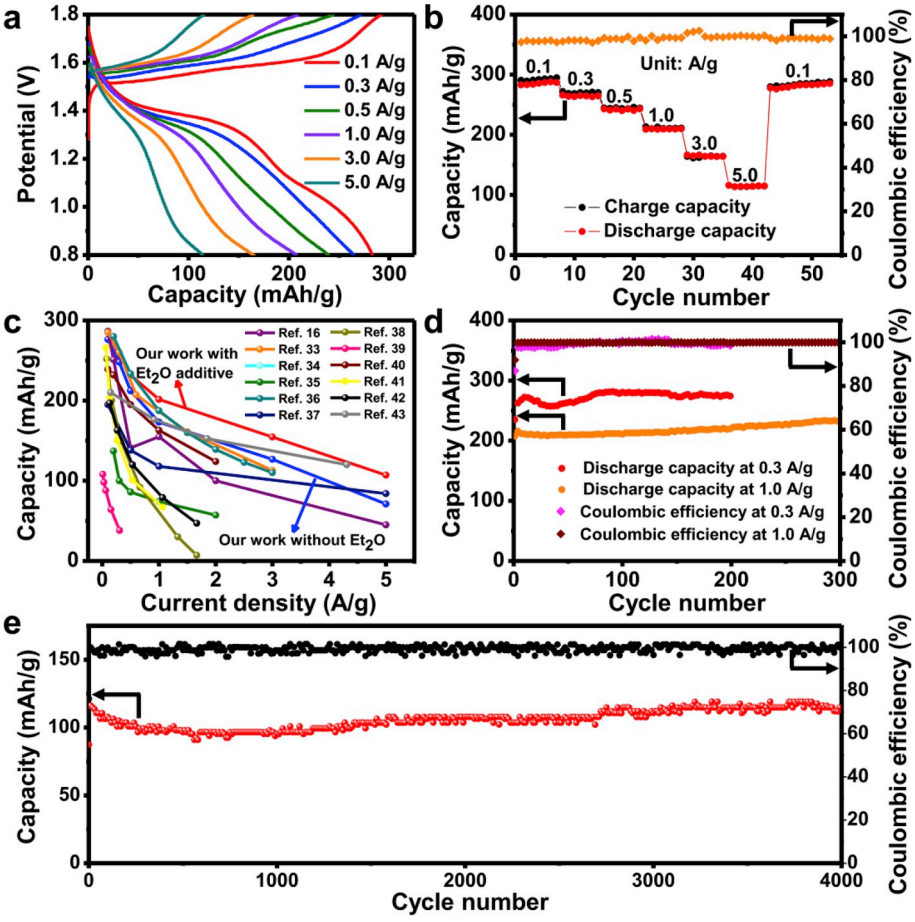

Fig. 2. Cycling stability and rate capability of Zn–MnO_2 battery: a, Galvanostatic charge-discharge curves of Zn–MnO_2 battery with 2 vol% Et_2O additive at different current densities. **b,** The corresponding rate performance for Zn–MnO_2 battery with 2 vol% Et_2O additive. **c,** Comparison of the rate capability of Zn–MnO_2 battery with other reported Mn-based ARZIBs in mild aqueous electrolyte. **d,** Cycling performances of Zn–MnO_2 battery with Et_2O additive at 0.3 A/g and 1 A/g. **e,** Long-term cycling performance of Zn–MnO_2 battery with Et_2O additive at 5 A/g.

electrode-electrolyte interphase (Fig. 3c and d) [45]. Comparing the EIS spectra revealed that the initial R_{ct} values of both cells without and with Et_2O were similar. After 125 cycles, R_{ct} of the cell with Et_2O slightly increased; whereas a significant increase of R_{ct} was observed from the cell without Et_2O, deriving from the restricted charge diffusivity after the anode failed. This suggests that adding Et_2O as electrolyte additive could enhance the electrode-electrolyte kinetics. The morphology change of the cycled Zn anodes after 125 cycles was also examined by ex-situ SEM analysis. The cycled Zn anode in the presence of Et_2O maintained a relatively flat and smooth surface without obvious detrimental protrusions (Fig. 3e, Fig. S16a); while rough surface with numerous flake-like dendrites was observed on the one without Et_2O (Fig. 3f, Fig. S16b). The cross-sectional view of the Zn plates revealed that the cycled Zn anode with Et_2O had a much denser and smoother

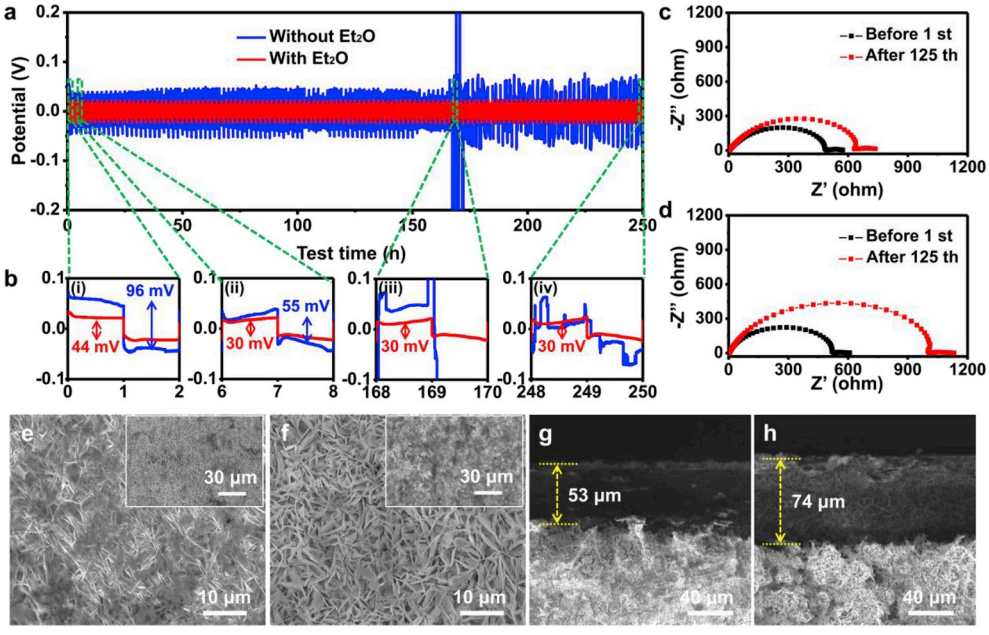

Fig. 3. Electrochemical characterizations of Zn–Zn symmetrical battery: a, Cyclic plating/stripping process of Zn–Zn symmetric cells with (red curve) and without (blue curve) Et_2O at a constant current density of 0.2 mA/cm^2. The plating/stripping capacity of each cycle was kept at 0.2 mAh/cm^2. **b,** Enlarged voltage profiles of the cells at different cycles. **c and d,** EIS plots of cycled Zn–Zn symmetric cells with (c) and without (d) Et_2O additive. **e and f,** Planar SEM images of Zn anode surface after 125 plating/stripping cycles obtained from Zn–Zn symmetrical cells at a capacity of 0.2 mAh/cm^2 with (e) and without (f) Et_2O additive. Insets are the panorama SEM images. **g and h,** Cross sectional images of Zn anode after 125 plating/stripping cycles with (g) and without (h) Et_2O additive.

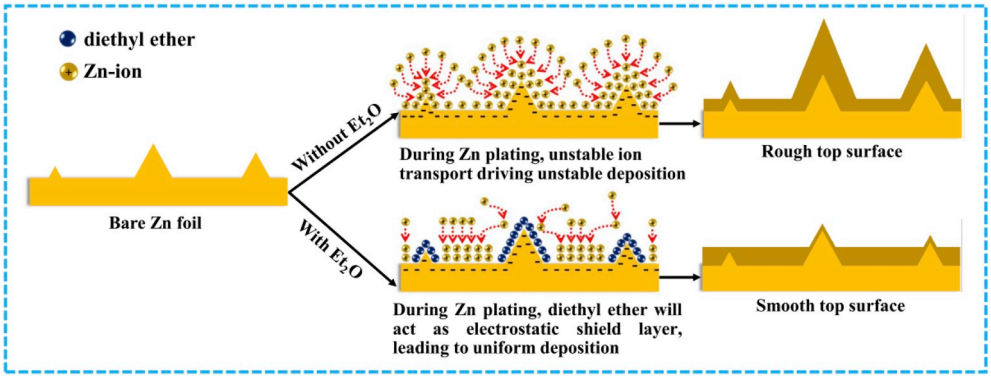

Fig. 4. Schematics of morphology evolution for Zn anodes in mild aqueous electrolyte with and without Et_2O additive during Zn stripping/plating cycling.

feature with a thickness of only ~53 μm (Fig. 3g). Without Et_2O, the cycled Zn anode exhibited a porous microstructure and the thickness was ~74 μm (Fig. 3h). The compact Zn film with a smaller thickness could facilitate charge transport and result in the lower charge transfer resistance observed from the cells with Et_2O additives. XRD further confirmed that both zinc plating on Zn anode after plating/stripping cycles were Zn metals (Fig. S17). No $Zn(OH)_2$ or any other derivatives were captured in the XRD spectra. XPS spectra also revealed the presence of ether group (R-C-O-C-R') on the zinc anode surface after cycling from cells with Et_2O (Fig. S18). After 90 s Ar^+ plasma treatment, the signal from the ether group was completely disappeared (Fig. S19), suggesting that the Et_2O additives were only attached to the zinc surface.

Based on all above analyses, we proposed that Et_2O as electrolyte additive played a vital role on Zn deposition. As schematically shown in Fig. 4, before the deposition process, the zinc plate may exhibit some initial surface roughness. During deposition, under a certain electric bias, these extrusions tips would exhibit higher electric field strength, which induced the fastest ion deposition. This process was a typical dendrite growth mechanism in rechargeable batteries [23,46]. When a small amount of Et_2O presents in the electrolyte, the highly-polarized Et_2O molecules would also be preferably adsorbed on initial Zn tips driven by the highly local electric field. Adsorption of Et_2O would hinder further deposition of Zn^{2+} to the tip areas. As a result, the deposition of Zn^{2+} would be shifted to the flat region where had minimal Et_2O coverage. In this way, the initial morphological fluctuation could be diminished and the Zn plate would remain a flat surface during repeated cycling process. Furthermore, the 2 vol% concentration might be the appropriate quantity for Et_2O to just cover the dendrites. Less amount of Et_2O (e.g. 1 vol%) might not be enough to cover all the initial dendrites. Too much Et_2O (e.g. 3 vol%) might provide additional coverage on the flat region, and thus the preferred selective deposition of Zn on the flat area was suppressed.

4. Conclusion

In this work, we discovered that a small amount of Et_2O electrolyte additive could significantly suppress the formation of protrusions on Zn metal anode, which largely improved the cycling life of ARZIB. When 2 vol% Et_2O was added in the 3 M $Zn(CF_3SO_3)_2$ and 0.1 M $Mn(CF_3SO_3)_2$ aqueous electrolyte, the Zn–MnO_2 battery exhibited excellent performances in terms of high initial CE (95.6% at 50 mA/g), high rate capability (98.9% capacity recovery when current recovered to 0.1 A/g), and long-term cycling stability (high capacity retention of 97.7% at 5 A/g). This performance was significantly higher than the same one without Et_2O additive and also superior to other reported Mn-based ARZIBs in a mild aqueous electrolyte. The improvement performance was attributed to the preferred adsorption of Et_2O molecules on the protrusion tips, so that the Zn^{2+} deposition shifted to the other areas and flattened the Zn anode surface. This discovery may bring profound impacts toward the development of high-perform aqueous rechargeable battery by providing a facile and effective strategy for life cycle improvement.

Acknowledgements

This work is supported by National Science Foundation under Award #CMMI-1148919. W.X. thanks the financial support from the China Scholarship Council scholarship. C. Hu thanks the support from the Hightower Chair Foundation and NSFC (51572040) and the Fundamental Research Funds for the Central Universities (2018CDQYWL0046, 2019CDXZWL001). L. Mai thanks the support by the National Key Research and Development Program of China (2016YFA0202603), the Program of Introducing Talents of Discipline to Universities (B17034), the National Natural Science Foundation of China (51521001 and 51602239).

Appendix A. Supplementary data

Supplementary data to this article can be found online at https://doi.org/10.1016/j.nanoen.2019.05.042.

References

[1] P. Senguttuvan, S.D. Han, S. Kim, A.L. Lipson, S. Tepavcevic, T.T. Fister, I.D. Bloom, A.K. Burrell, C.S. Johnson, Adv. Energy Mater. 6 (2016) 1600826.
[2] P. Canepa, G. Sai Gautam, D.C. Hannah, R. Malik, M. Liu, K.G. Gallagher, K.A. Persson, G. Ceder, Chem. Rev. 117 (2017) 4287–4341.
[3] W. Xu, S. Dai, G. Liu, Y. Xi, C. Hu, X. Wang, Electrochim. Acta 203 (2016) 1–8.
[4] K. Zhao, L. Zhang, R. Xia, Y. Dong, W. Xu, C. Niu, L. He, M. Yan, L. Qu, L. Mai, Small 12 (2016) 588–594.
[5] R. Trócoli, F. La Mantia, ChemSusChem 8 (2015) 481–485.
[6] M.H. Alfaruqi, V. Mathew, J. Song, S. Kim, S. Islam, D.T. Pham, J. Jo, S. Kim, J.P. Baboo, Z. Xiu, Chem. Mater. 29 (2017) 1684–1694.
[7] S. Islam, M.H. Alfaruqi, V. Mathew, J. Song, S. Kim, S. Kim, J. Jo, J.P. Baboo, D.T. Pham, D.Y. Putro, J. Mater. Chem. 5 (2017) 23299–23309.
[8] M.H. Alfaruqi, V. Mathew, J. Gim, S. Kim, J. Song, J.P. Baboo, S.H. Choi, J. Kim, Chem. Mater. 27 (2015) 3609–3620.
[9] I. Arise, S. Kawai, Y. Fukunaka, F. McLarnon, J. Electrochem. Soc. 160 (2013) D66–D74.
[10] I. Arise, T. Homma, F. McLarnon, Y. Fukunaka, ECS Trans. 35 (2011) 3–9.
[11] Z. Liu, G. Pulletikurthi, A. Lahiri, T. Cui, F. Endres, Dalton Trans. 45 (2016) 8089–8098.
[12] S. Thomas, N. Birbilis, M. Venkatraman, I. Cole, Corrosion, J. Sci. Eng. 68 (2012) 015001–015009.
[13] K.E. Sun, T.K. Hoang, T.N.L. Doan, Y. Yu, X. Zhu, Y. Tian, P. Chen, ACS Appl. Mater. Interfaces 9 (2017) 9681–9687.
[14] S. Higashi, S.W. Lee, J.S. Lee, K. Takechi, Y. Cui, Nat. Commun. 7 (2016) 11801.
[15] Z. Liu, T. Cui, G. Pulletikurthi, A. Lahiri, T. Carstens, M. Olschewski, F. Endres, Angew. Chem. Int. Ed. 55 (2016) 2889–2893.
[16] K. Zhao, C. Wang, Y. Yu, M. Yan, Q. Wei, P. He, Y. Dong, Z. Zhang, X. Wang, L. Mai, Adv. Mater. Interfaces 5 (2018) 1800848.
[17] L. Kang, M. Cui, F. Jiang, Y. Gao, H. Luo, J. Liu, W. Liang, C. Zhi, Adv. Energy Mater. 8 (2018) 1801090.
[18] D. Chao, C. Zhu, M. Song, P. Liang, X. Zhang, N.H. Tiep, H. Zhao, J. Wang, R. Wang, H. Zhang, Adv. Mater. 30 (2018) 1803181.

[19] J.F. Parker, C.N. Chervin, I.R. Pala, M. Machler, M.F. Burz, J.W. Long, D.R. Rolison, Science 356 (2017) 415–418.
[20] G.G. Yadav, J.W. Gallaway, D.E. Turney, M. Nyce, J. Huang, X. Wei, S. Banerjee, Nat. Commun. 8 (2017) 14424.
[21] G.G. Yadav, X. Wei, J. Huang, J.W. Gallaway, D.E. Turney, M. Nyce, J. Secor, S. Banerjee, J. Mater. Chem. 5 (2017) 15845–15854.
[22] K. Xu, Chem. Rev. 114 (2014) 11503–11618.
[23] F. Ding, W. Xu, G.L. Graff, J. Zhang, M.L. Sushko, X. Chen, Y. Shao, M.H. Engelhard, Z. Nie, J. Xiao, J. Am. Chem. Soc. 135 (2013) 4450–4456.
[24] K. Abraham, J. Goldman, D. Natwig, J. Electrochem. Soc. 129 (1982) 2404–2409.
[25] W. Xiao, D. Wang, X.W. Lou, J. Phys. Chem. C 114 (2009) 1694–1700.
[26] W. Xu, Z. Jiang, Q. Yang, W. Huo, M.S. Javed, Y. Li, L. Huang, X. Gu, C. Hu, Nano Energy 43 (2018) 168–176.
[27] K. Zhao, C. Sun, Y. Yu, Y. Dong, C. Zhang, C. Wang, P.M. Voyles, L. Mai, X. Wang, ACS Appl. Mater. Interfaces 10 (2018) 44376–44384.
[28] S. Islam, M.H. Alfaruqi, V. Mathew, J. Song, S. Kim, S. Kim, J. Jo, J.P. Baboo, D.T. Pham, D.Y. Putro, Y.-K. Sun, J. Kim, J. Mater. Chem. 5 (2017) 23299–23309.
[29] C. Xu, B. Li, H. Du, F. Kang, Angew. Chem. Int. Ed. 51 (2012) 933–935.
[30] H.L. Pan, Y.Y. Shao, P.F. Yan, Y.W. Cheng, K.S. Han, Z.M. Nie, C.M. Wang, J.H. Yang, X.L. Li, P. Bhattacharya, K.T. Mueller, J. Liu, Nature Energy 1 (2016).
[31] O. Delmer, P. Balaya, L. Kienle, J. Maier, Adv. Mater. 20 (2008) 501 +).
[32] K.F. Zhong, B. Zhang, S.H. Luo, W. Wen, H. Li, X.J. Huang, L.Q. Chen, J. Power Sources 196 (2011) 6802–6808.
[33] H. Pan, Y. Shao, P. Yan, Y. Cheng, K.S. Han, Z. Nie, C. Wang, J. Yang, X. Li, P. Bhattacharya, Nature Energy 1 (2016) 16039.
[34] B. Jiang, C. Xu, C. Wu, L. Dong, J. Li, F. Kang, Electrochim. Acta 229 (2017) 422–428.
[35] N. Zhang, F. Cheng, J. Liu, L. Wang, X. Long, X. Liu, F. Li, J. Chen, Nat. Commun. 8 (2017) 405.
[36] J. Huang, Z. Wang, M. Hou, X. Dong, Y. Liu, Y. Wang, Y. Xia, Nat. Commun. 9 (2018).
[37] D. Xu, B. Li, C. Wei, Y.-B. He, H. Du, X. Chu, X. Qin, Q.-H. Yang, F. Kang, Electrochim. Acta 133 (2014) 254–261.
[38] M.H. Alfaruqi, J. Gim, S. Kim, J. Song, D.T. Pham, J. Jo, Z. Xiu, V. Mathew, J. Kim, Electrochem. Commun. 60 (2015) 121–125.
[39] S.-D. Han, S. Kim, D. Li, V. Petkov, H.D. Yoo, P.J. Phillips, H. Wang, J.J. Kim, K.L. More, B. Key, Chem. Mater. 29 (2017) 4874–4884.
[40] J. Hao, J. Mou, J. Zhang, L. Dong, W. Liu, C. Xu, F. Kang, Electrochim. Acta 259 (2018) 170–178.
[41] M.H. Alfaruqi, S. Islam, V. Mathew, J. Song, S. Kim, D.P. Tung, J. Jo, S. Kim, J.P. Baboo, Z. Xiu, Appl. Surf. Sci. 404 (2017) 435–442.
[42] M.H. Alfaruqi, S. Islam, J. Gim, J. Song, S. Kim, D.T. Pham, J. Jo, Z. Xiu, V. Mathew, J. Kim, Chem. Phys. Lett. 650 (2016) 64–68.
[43] C. Xu, B. Li, H. Du, F. Kang, Angew. Chem. Int. Ed. 51 (2012) 933–935.
[44] Y. Fu, Q. Wei, G. Zhang, X. Wang, J. Zhang, Y. Hu, D. Wang, L. Zuin, T. Zhou, Y. Wu, Adv. Energy Mater. 8 (2018) 1801445.
[45] K. Zhao, M. Wen, Y. Dong, L. Zhang, M. Yan, W. Xu, C. Niu, L. Zhou, Q. Wei, W. Ren, Adv. Energy Mater. 7 (2017) 1601582.
[46] Y. Sawada, Phys. Stat. Mech. Appl. 140 (1986) 134–141.

Weina Xu is a Ph.D. student in Chongqing University. She carried out his visiting scholar research in the laboratory of Prof. Xudong Wang at University of Wisconsin-Madison in 2017–2019. Her research interests are mainly focused on synthesis and applications of functional nanomaterials for energy storage devices and sensors.

Kangning Zhao is currently Assistant Professor of Institute for Sustainable Energy at Shanghai University. He received his Ph.D. degree from Wuhan University of Technology in 2019. He carried out his visiting scholar research in the laboratory of Prof. Xudong Wang at the University of Wisconsin-Madison in 2016–2018. Currently, his research interest includes electrochemical catalysis and energy storage devices.

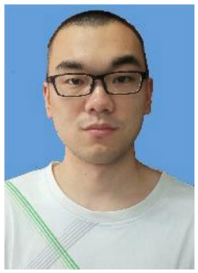

Wangchen Huo is a Ph.D. student in Chongqing University. His research interests are related to the design and application of nanomaterial for photocatalysis and supercapacitors.

Yizhan Wang received Ph.D. degree in Polymer Chemistry and Physics from Jilin University in 2013. Yizhan joined Prof. Xudong Wang's group as a postdoctoral fellow at University of Wisconsin-Madison in March, 2017. His current research focuses on ionic liquid epitaxy growth of functional oxides.

Guang Yao is a Ph.D. student in University of Electronic Science and Technology of China. His major is microelectronics and solid-state electronics. His research interests include design and fabrication of flexible electronic devices, such as wearable biomedical devices.

Xiao Gu graduated from Dept. of Physics in Fudan University 2002 and received his Ph.D. degree in 2007 from Fudan University. He was postdoctoral researcher at University of British Columbia, Vancouver, Canada from 2007 to 2009. From 2010 to 2014, he worked as research associate in Dept. of Environmental Sciences and Engineering of Fudan University. Now he is research professor in Dept. of Applied Physics in Chongqing University. His research interests cover advanced materials, such as energy materials (lithium ion battery, supercapacitors, solar cell) and functional materials such as catalysts etc.

Hongwei Cheng is a professor of metallurgical physical chemistry at the School of Materials Science and Engineering, Shanghai University. He received his Ph.D. in Metallurgical Engineering from Shanghai University in 2009. He worked as a visiting scholar at the University of Wisconsin-Madison in 2018. His research interests include oxygen permeable membranes, solid electrolytes, electrode materials and their applications.

Liqiang Mai is Chair Professor of Materials Science and Engineering at Wuhan University of Technology (WUT). He received his Ph.D. from WUT in 2004. He carried out his postdoctoral research in the laboratory of Prof. Zhonglin Wang at Georgia Institute of Technology in 2006–2007 and worked as advanced research scholar in the laboratory of Prof. Charles M. Lieber at Harvard University in 2008–2011. His current research interests focus on nanowire materials and devices for energy storage. He received the National Natural Science Fund for Distinguished Young Scholars, the First Prize for Hubei Natural Science Award and so forth.

Chenguo Hu is a professor of physics in Chongqing University and the director of Key Lab of Materials Physics of Chongqing Municipality. She received her Ph.D. in Materials from Chongqing University in 2003. Her research interests include methodology of synthesizing functional nanomaterials, design and fabrication of electronic devices, such as nanogenerators and sensors.

Xudong Wang is a professor in the department of Materials Science and Engineering at University of Wisconsin–Madison. He received his PhD degree in Materials Science and Engineering from Georgia Tech in 2005. His current research interests include developing advanced nanomaterials and nanodevices for mechanical energy harvesting from human activities for biomedical applications; understanding the coupling effect between piezoelectric polarization and semiconductor functionalities; and studying the growth mechanisms and developing assembly techniques of oxide nanostructures. He is the author of more than 130 publications and holds more than 10 patents on oxide and piezoelectric materials processing and applications.